# Tribological analysis of TiN film during run-in period: An in situ investigation under controlled environment in eSEM

Aslihan Sayilan, Nicolas Mary, David Philippon, Philippe Steyer, Sylvie Descartes

# Tribological Analysis of TiN film during Run-in Period: An *in situ* Investigation Under Controlled Environment in eSEM

Aslihan SAYILAN[1,2], Nicolas MARY[1], David PHILIPPON[2], Philippe STEYER[1*], Sylvie DESCARTES[2*]

[1]Univ. Lyon, INSA-Lyon, CNRS UMR 5510, MATEIS, F-69621 Villeurbanne, France

[2]Univ. Lyon, INSA-Lyon, CNRS UMR5259, LaMCoS, F-69621 Villeurbanne, France

**corresponding authors*

**Abstract**

Most of the conventional tribological studies are performed through long duration tests, which therefore often neglect the run-in period. To highlight these early stages of damaging, which may present a predominant role on the global wear, a **custom-built** dedicated mini-tribometer in a linear reciprocating configuration was designed and is presented in the paper. The tribometer is developed to be implemented into an environmental SEM, in which the atmosphere is controlled. As a proof-of-concept, a well-known model system steel-hard TiN coating is used for two different atmospheres: vacuum and humid environments. The adopted small-scale and *in situ* approach has led to the validation of the mini-tribometer. Through this combined strategy, some scenarios of materials degradation are suggested in light of the interface nature involved in the contact. In this sense, the role of the environment is pointed out, and explained.

**Highlights:**

- A custom-built tribometer was designed to be implemented into an environmental SEM.
- A TiN PVD coating was used as the model surface.
- An *in situ* small scale characterization of the early stage of damaging was done throughout the test.
- Humidity favors the growth of a passive layer acting as a solid lubricant.
- Wear behavior is governed by the dynamics of debris, influenced by the contact environment.

**Keywords:** environmental SEM; tribology; titanium nitride; *in situ*; run-in; humidity

## Introduction

Tribology is a multidisciplinary science focused on the dynamic study of a system composed of two surfaces in contact [1]. The tribological system can be defined by three main components: i) the nature of the contact, depending on its geometry, on the different materials involved and on their surface properties, ii) the rubbing conditions, linked to the dynamic parameters (load, stress, time, speed…), and iii) the environment of the contact zone, associated with atmosphere, temperature and the stiffness of the device containing the contact [2, 3]. Therefore, many parameters may influence the wear behavior of materials, so that it is often complex to assess the tribological response of surfaces [3].

From a technological viewpoint, tribometer systems which have a pin or ball counter-face over a flat surface (pin or ball-on-disk, pin or ball-on plate system) are commonly used. Those can be classified into two main different categories regarding their kinematics: rotational tribometers, which have a rotational actuator, and the reciprocating tribometers, which have an oscillating actuator. The selection of the proper type of tribometer is governed by the final targeted application [4].

Normally, the films on rigid substrates have a significant place in people's every-day lives as the coatings for numerous devices and applications. It is needed to consider that the functionality of these films in terms of their mechanical, electrical, magnetic properties are usually driven from the small dimensions [5]. Additionally, the wear procedure and the material response are mostly analyzed for lab duration tests at a large scale, through a conventional *post-mortem* comparative approach. However, for small-scale engineering devices such as MEMs and NEMs, an adapted small-scale analysis of the contact is required, which was on the basis of micro-tribology [6]. Additionally, Kumar et al. [7] pointed out the micrometer-sized phenomena which is linked to small-scale surface properties (*e.g.* surface energy, roughness). Also, the range of the normal load and the size of the contact have, in particular, to be adapted

[8]. Recently, there is a considerable interest in examining the micro and nano-scale frictional contacts in the field of micro-and nano-sized devices, or to better understand the role of the asperities in macro-scale [9]. Testing procedures in terms of both loads and contact sizes have to be adjusted, together with the investigation methods involving physical and chemical complementary analyses [9-11].

For a small-scale tribological characterization, two main types of tribometers are reported in the literature. It can be found nanotribometers, which derive from AFM-based systems. They are devoted to weakly defective surfaces such as in the electronics field [4]. AFMs with nano-tribometers can be used for the tribological analysis of small-scale engineering devices. To perform in situ tribological analysis in small-scale, AFM is an efficient choice regarding its high resolution and high precision on measurement abilities. Also, nano-tribometers can be used by coupling with electron microscopes to perform *in situ* analysis. For example, Deasi et *al.* [12] developed a nano-tribometer which provides dynamic investigation of tribological behavior of materials to be used for MEMs for the load range 1-100 nN. The second class of tribometers is called micro-tribometers, which are operable in vacuum or ambient air conditions with micro and milli-newton normal load ranges. Here, nano-indenters with AFM or FFM (friction for microscopy) could provide the tribological analysis from nano to micro scale load ranges [7]. Moreover, to better understand the complex surface/counter-face/environment interaction, *in situ* approaches of characterization are recommended, giving the access to a detailed evaluation of the friction nature throughout the phenomenon. It is then possible to follow the wear track and friction evolution at every cycle, during the entire process, and with well-defined contact conditions. Dynamic of the contact is then considered from a (micro)structural point of view by light, electron, or atomic force microscopes [13-20], and/or from a chemical point of view through Raman, XPS, AES spectroscopies [21-24]. For instance, Murarash et *al.* [25] examined the tribological behavior of biological surfaces by visual

inspection *in situ* conditions by operating the tribometer in SEM chamber. Here, the developed tribometer for these particular surfaces has flat-on-flat contact to examine the pulling-off, shear and/or the peeling off the surfaces.

Also, Naerheim [26] developed a tribometry system which is implementable into a dedicated test chamber. The latter is equipped with scanning electron microscopy facilities, an Auger electron spectroscope (AES), a small-area multichannel X-ray photoelectron spectroscope (XPS) and a mass spectrometer. This system was based on having a cylinder and pin contact at the same time and tribometer could be operated in rolling or sliding mode for *in situ* analysis. In another research, to examine the role of environmental conditions, Meylan et *al.* [27] developed a ball-on-disk tribometer to couple with digital holographic microscope and to operate in high temperature and high vacuum conditions.

The long-term tribological behavior of materials is well-documented in general. [17, 28-31]. However, changes on the roughness, grain size or texture of the surface based on the frictional contact mostly occur during run-in period which affects the friction coefficient [32, 33]. The variations on friction coefficient at run-in period is based on contaminations on the film surface, formation of oxide layer, transferred material reaction of lubricants or reorientation of the sub-surface microstructure during the contact [30]. Thus, the presented approach in this paper involves a dedicated custom-built mini-tribometer, which was developed to examine the early stages of the contact. To prove the reliability of the tribometer, the system has been selected on a model hard surface: titanium nitride. TiN films are indeed well known for a long time for their enhanced tribo-chemical properties [22]. They are used in small-scale engineering applications such as ohmic contacts for Schottky barriers [23], solar cells, NEMs, MEMs [7], and anti-wear applications such as cutting tools, and orthopedic implants or bearings [22]. However, the performance of TiN films is sensitive to the tested atmosphere: vacuum environment [34, 35], water vapor [36-38], oxygen [39] or nitrogen [35]. For example, Yoon et *al.* [37] studied the

wear character of TiN films against a steel ball from 2% to 25% and 85% relative humidity levels. It was pointed out that, for a long test (30000 cycles), the coefficient of friction decreased with the increasing relative humidity based on the formation of $TiO_2$ on the film surface. Besides, the structure of the worn coating was analyzed by Gant *et al.* [38] under different relative humidity environments with Raman spectroscopy. They demonstrated that high relative humidity promoted the rutile phase formation, whereas the anatase phase mostly predominated at lower humidity levels. In order to assess the effect of the atmosphere on the tribological behavior for the small-scale analysis of the contact, the presented mini-tribometer was designed to be implemented into the chamber of an environmental SEM (eSEM), in which atmosphere of the contact can be controlled, and chemical information can be obtained. In the current paper, modification of the relative humidity will be the variable key-parameter. In this sense, the presented mini-tribometer represents a step ahead with respect to existing systems involving light microscopes or conventional SEMs [40].

This paper proposes an *in situ* approach at the meso-scale, to investigate the tribological behavior of a material during the run-in period, highlighting the effect of the contact environment. The mini-tribometer, the TiN film, and the environmental SEM are first described. Both qualitative and quantitative results are then given by considering the coated flat sample as well as the ball counterpart. Results are finally discussed in light of the debris dynamic on the one hand, and the effect of the humidity on the other hand.

## 2. Materials and Methods

### 2.1 Mini-Tribometer in ESEM

The mini-tribometer is a custom-built device that is based on a reciprocating ball-on-plate setup. A 3-axes sensor allows to measure normal ($F_z$), tangential ($F_x$) and lateral force ($F_y$). The range for the force on x and y axes is from -50N to 50 N while for z-axis the range is from 0N to 50N.

The sliding velocity can be set between 0.5 to 2 mm/s. Two motors are controlling the position of the counter-face. While the main motor provides the sliding motion along the x-axis, the rotational one controls the loading and unloading of the contact by moving the sliding arm along the z-axis. The ball counter-face is inserted into the sliding arm, which is placed on the upper part of the mini-tribometer. Moving the arm alternatively along the x-direction, the counter-face moves over the surface of the sample along ±20 mm, and its position is controlled by a Labview-based software developed in the laboratory. Time, displacement and the number of cycles is also recorded (Figure 1a). The device provides to set and control the temperature of the system to the desired value with ±0.1°C precision thanks to its temperature sensor and Peltier elements located under the flat sample.

The mini-tribometer is compact to be implementable in the eSEM chamber, and could be used under high vacuum as well as under different environmental conditions (*e.g.* different relative humidity, gas nature, and temperatures). By implementing the tribometer into the eSEM chamber (Figure 1), small-scale characterizations can be performed without modifying the atmosphere containing the contact. In high vacuum Secondary Electrons (SE) detector (i.e. Everhart-Thornley detector) and back-scattering electrons (BSE) detector can be used; with a gas pressure in the chamber gaseous secondary electrons detector (GSED) or Large field detector (LF) can be used. The used SEM-Quattro (Thermo Fisher Scientific) is a high-resolution scanning electron microscope, which is able to operate not only in high vacuum but also in controlled gaseous environments. Furthermore, the hygrometry surrounded the contact can be controlled by modifying the flat sample temperature (use of cooling Peltier elements) and the water vapor pressure $P_{H_2O}$ inside the SEM chamber [41].

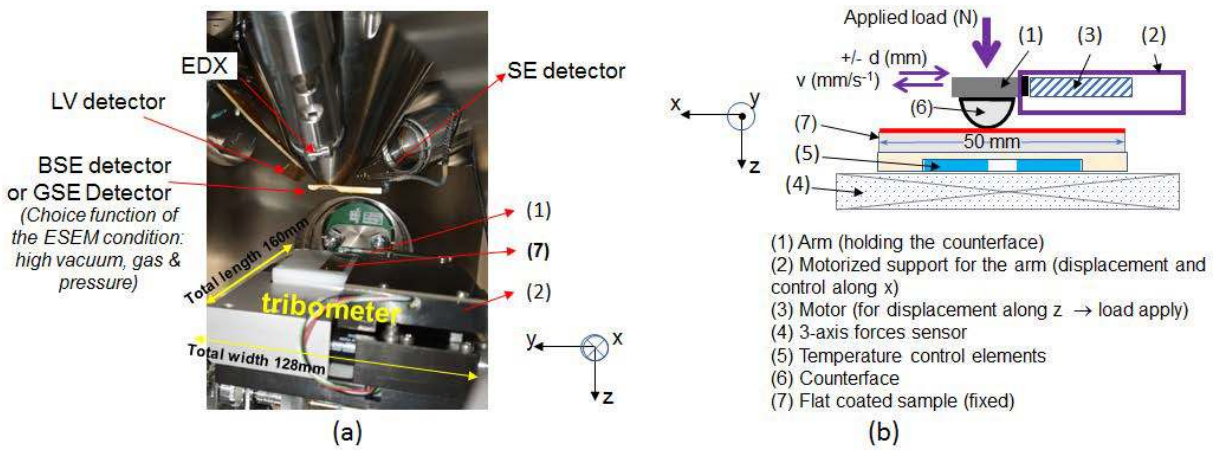


Figure 1: The mini-tribometer. a) Implementation inside the eSEM chamber, and b) Schema

## 2.2. Materials and contact conditions

Substrates were prepared as 12 mm in width, 50 mm in length and 2 mm in thickness to fit the dimensions of the sample requested for the tribometer. 2.3 µm-thick TiN films were deposited onto a mirror-polished mild steel substrate by the cathodic arc evaporation (CAE) process. As expected, the film presents the conventional fcc-TiN phase, with the classical heterogeneous microstructure obtained by CAE, gathering some pinholes pores, and droplets (Figure 2) [42-44]. More details on the film characteristics can be found in a previous dedicated paper [45].

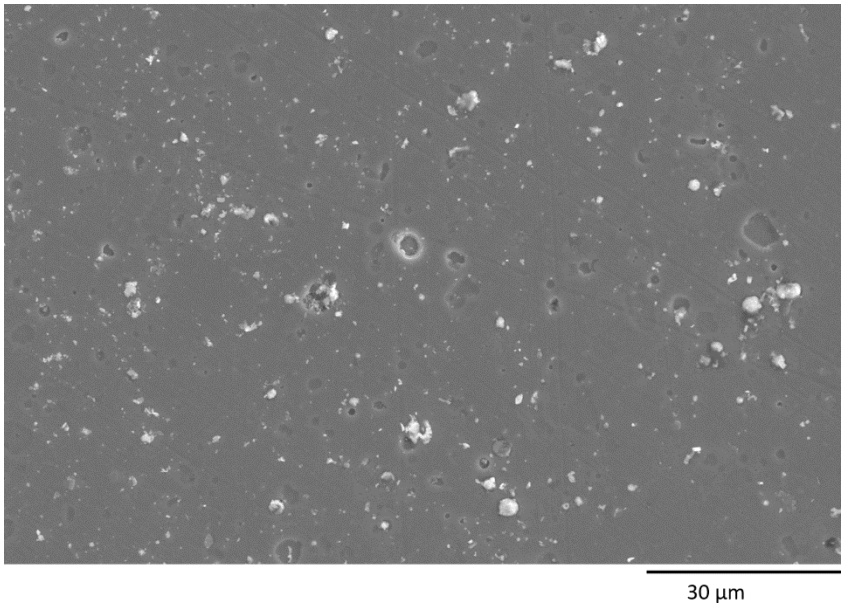


Figure 2: TiN film – SE image of the pristine surface

The applied normal load was 6 N and it was applied along 2 mm of displacement length, with a 1 mm/s sliding speed. The Young's modulus of TiN film was measured at 305 GPa [43], in good agreement with literature data [46, 47]. A steel ball (AISI52100) with a 10 mm diameter was selected as the counter-face. By considering the materials' mechanical properties and contact conditions, the maximum Hertz contact pressure was calculated as 1130 MPa.

2.3. *In situ* analysis

The whole tests were performed according to the procedure reported in Figure 3. A reduced number of cycles (100) was deliberately chosen to focus on the run-in period.

Preliminary tests were performed to select the best parameters (total number of cycles and periodicity of sets of cycles) leading to significant changes of the surface. To perform *in situ* analysis, sliding was interrupted and the contact was unloaded after every 10 cycles. That allows SEM captions of the worn zone, thus, to assess the wear track modifications. Two regions of interest were specifically monitored along the wear track: one edge of the track (turning point) and its center (where the sliding speed is constant). The unloading-loading edge was not analyzed during the *in situ* tests.

Tests were performed in two different environments: under high vacuum ($10^{-4}$ Pa) and in water vapor environment (50% relative humidity). For the targeted 50% relative humidity, the saturated water vapor pressure $P_{H_2O}$ in the SEM chamber and the coated sample temperature were set to 400 Pa and 4°C respectively.

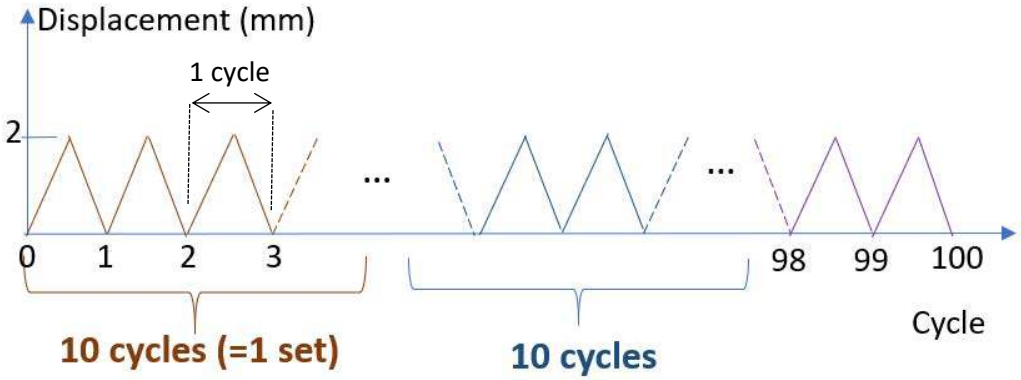


Figure 3: Protocol for *in situ* tribological tests

2.4. *Post-mortem* analysis

The mini-tribometer as coupled with microscope could provide to perform in situ analysis on the flat; however, not for the ball surface. Thereby, it was not possible to analyse the wear tracks on the balls after every ten cycles without venting the chamber. Since the tests were carried out in controlled environment, only *post-mortem* analysis (after 100 cycles) was done on the ball surfaces.

Also, on the wear tracks TiN films, three regions of interests were investigated in *post mortem* conditions by energy dispersive x-ray spectroscopy (EDS). An Oxford Ultim max 100 spectrometer was used to analyse the debris and characterise the transferred film. For those chemical analyses, Energy resolution was selected as 1024 channels, while the process time was determined as 3 and dwell time was 300 µs. Analyses were carried out at an accelerating voltage of 10 kV, for a working distance of 8.6 mm and a dwell time of 300µs.

Surface profile analysis was performed both on the ball and on the TiN-coated steel to estimate their worn volumes. Surface morphologies of the wear tracks and balls were extracted using a ZeGage Pro non-contact scanning interferometer from Zygo company. Mx$^{TM}$ software integrated with interferometer also provides 3D mapping. In this study, the Mountain software was used to extract the surface profiles and to calculate the wear volumes. The average wear

volume was calculated by the integral method from ten profiles obtained from different regions along the whole wear track region.

## 3. Results

### 3.1. *In situ* analysis

Figure 4 shows examples of the tangential force evolution after different number of cycles. During each cycle the tangential force is constant for both atmospheres. The tangential force evolution for the forward and backward displacement is similar. The applied normal force is constant for each cycle and equal to the target value. The elasticity of the system and the stiffness of the arm allows a possible movement due to the interface evolution, *e.g.* the applied load might vary but in a very limited range.

An average friction coefficient was calculated for each reciprocating cycle (COF) when the speed is constant. Thus, the recorded data from turning points was omitted for the friction coefficient calculations. (approximately 12 % at each track end). The friction coefficient is defined as the ratio between the tangential force to the applied normal force.

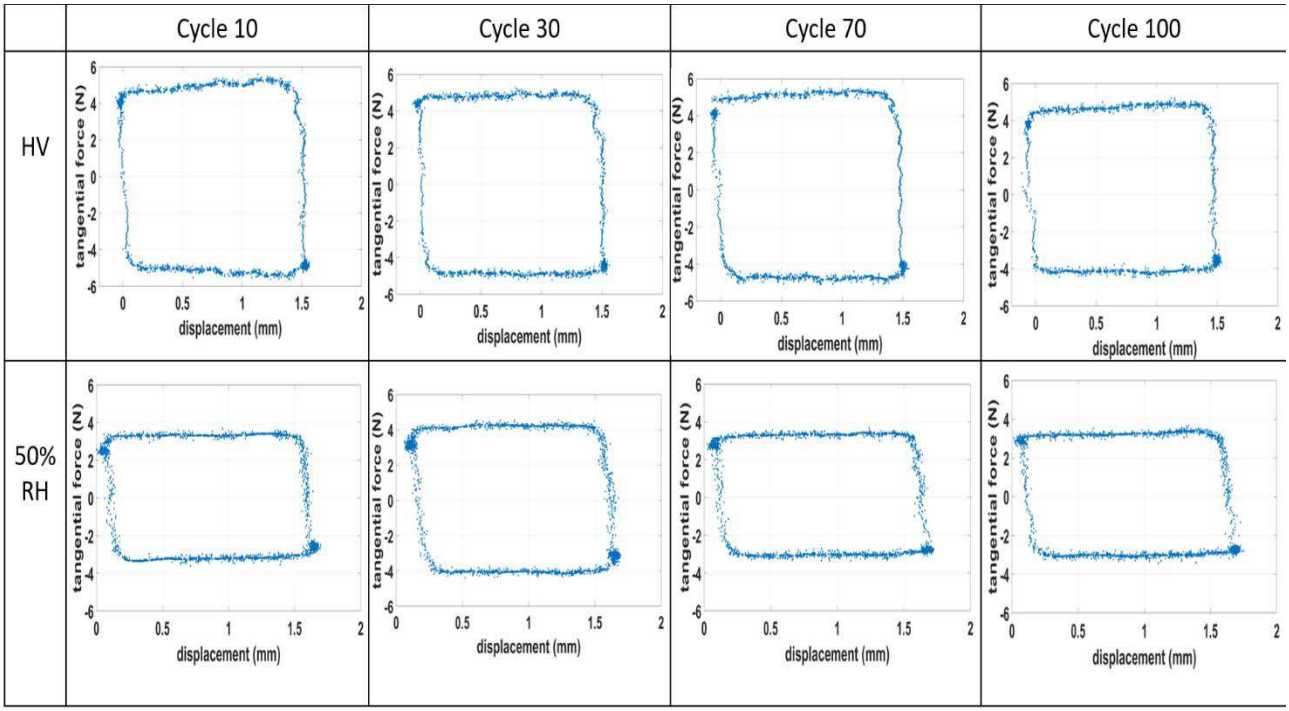

Figure 4: Tangential force *vs* displacement at different cycle (a) under high vacuum, (b) under RH 50%

Friction tests were monitored by plotting COF as a function of the cycle number (Figure 5) for both high vacuum and humid environment. A general interpretation of curves allows concluding that the COF evolutions are similar whatever the environments, with an increase during the first 30 cycles with a higher amplitude at high vacuum (0.90) than for humid conditions (0.55). Then, a similar slow decrease of the COF is recorded down to 0.67 and 0.47 for the high vacuum test and humid test respectively. The mean COFs for 100 cycles were calculated as 0.75 (±0.09) and 0.49 (±0.03) for the tests performed in high vacuum and 50% relative humidity respectively.

It is seen that the first cycle of each set systematically presents a lower coefficient of friction with respect to the other following 9 cycles in the same set. When the contact was reloaded and the sliding was restarted, there was a sharp drop of COF values, phenomenon met every 10 cycles.

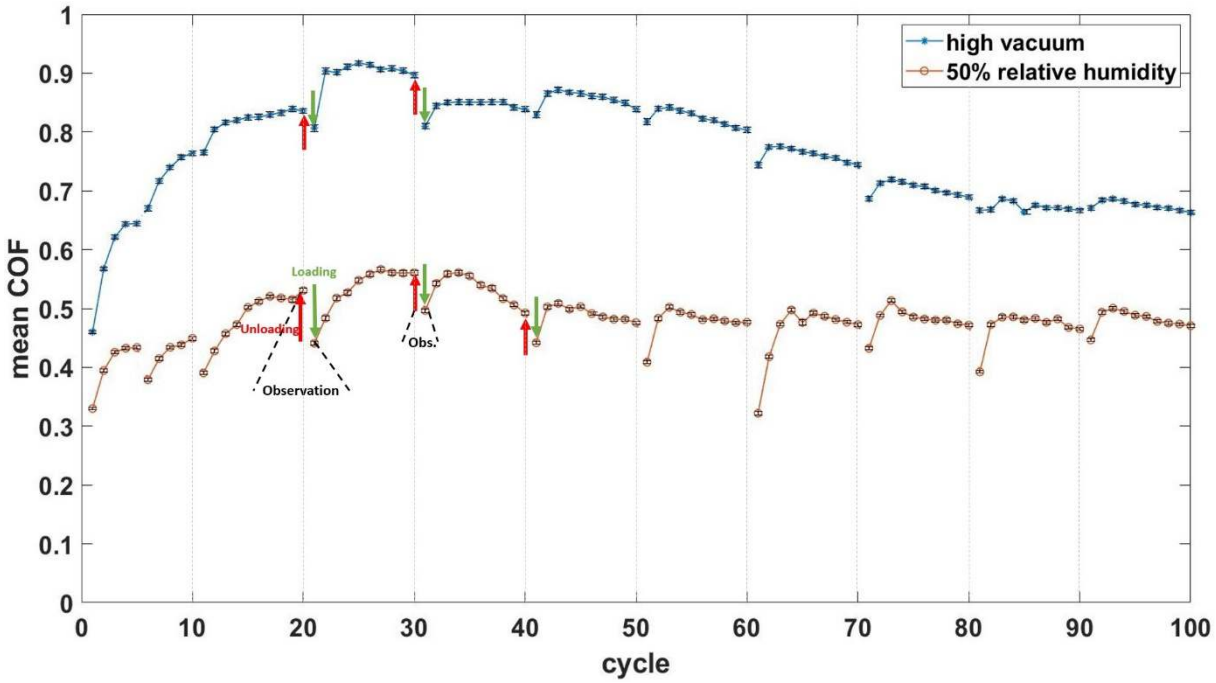


Figure 5: Mean coefficient of friction per cycle for the tests performed at high vacuum and 50% relative humidity

In addition to quantitative evaluation of the sliding via COF analysis, a complementary observation of the surface throughout the test was performed. SEM images were analyzed at low magnification in two specific regions of interest which are the center and the end of the wear track (Figure 6). It appears that whatever the environment, tracks are mainly identified by the debris left at its edges.

In both atmospheres, it is worth to mention that there was not a significant change observed between cycle 30 and cycle 40. In this sense, the highest COF value revealed after 30 cycles could be a consequence of particles sticking between the ball and the film surface.

In comparison with powder-like debris encountered under vacuum, the dynamic of debris generated under humidity seemed strongly changed, with a smoother track, in addition to fine and aligned debris. Moreover, the amount of debris observed at the edges is increasing with the test duration in humid environment.

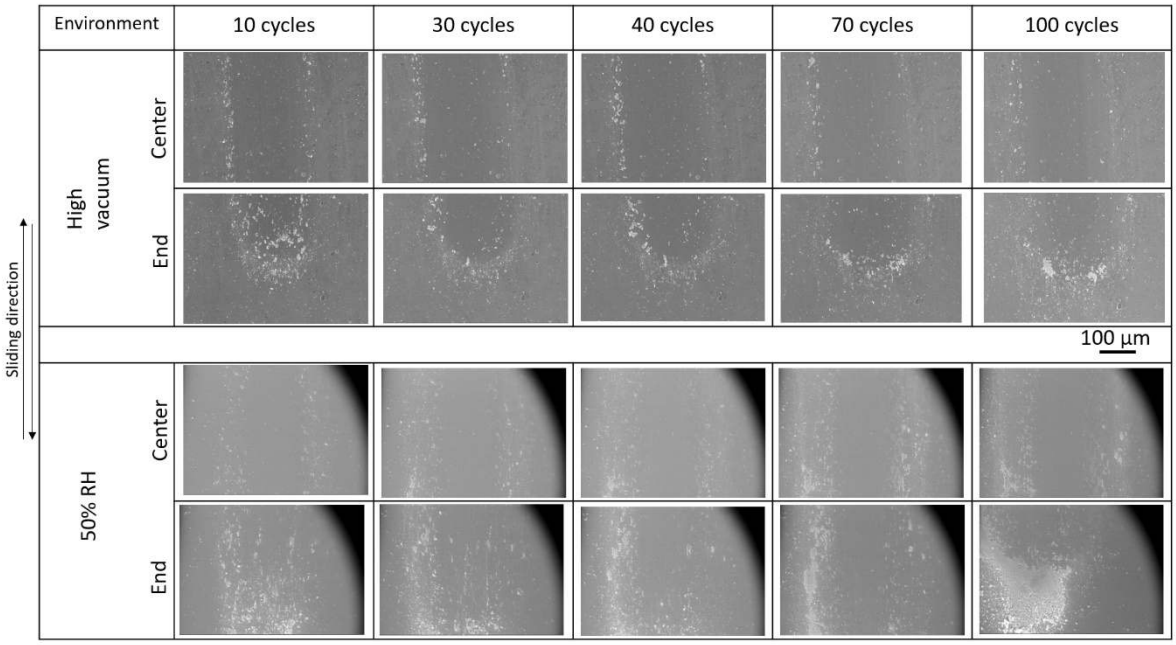


Figure 6: Images of wear tracks (center and end) at several numbers of cycles for the two environments (*NB*: *due to the gaseous secondary electron detector used for the humid mode, the aperture appears in images (top right) at low magnification*)

At higher magnification, in the case of high vacuum, the pores observed on the pristine surface (Figure 2) were still visible in the center of the friction track, after each 10 cycles set (red arrows in figure 7). After 10 cycles one can note the low flow of materials (e.g. highlighted by yellow arrows or circled by a dotted line), but this tends not to be visible afterwards. On the contrary, at 50% of relative humidity, the pores were gradually “disappearing” (red arrows on figure 8). On the same time, one can note that third body spread on the surface and the formation of agglomerates between 70 and 100 cycles in humid environment (yellow arrows and dotted ellipse).

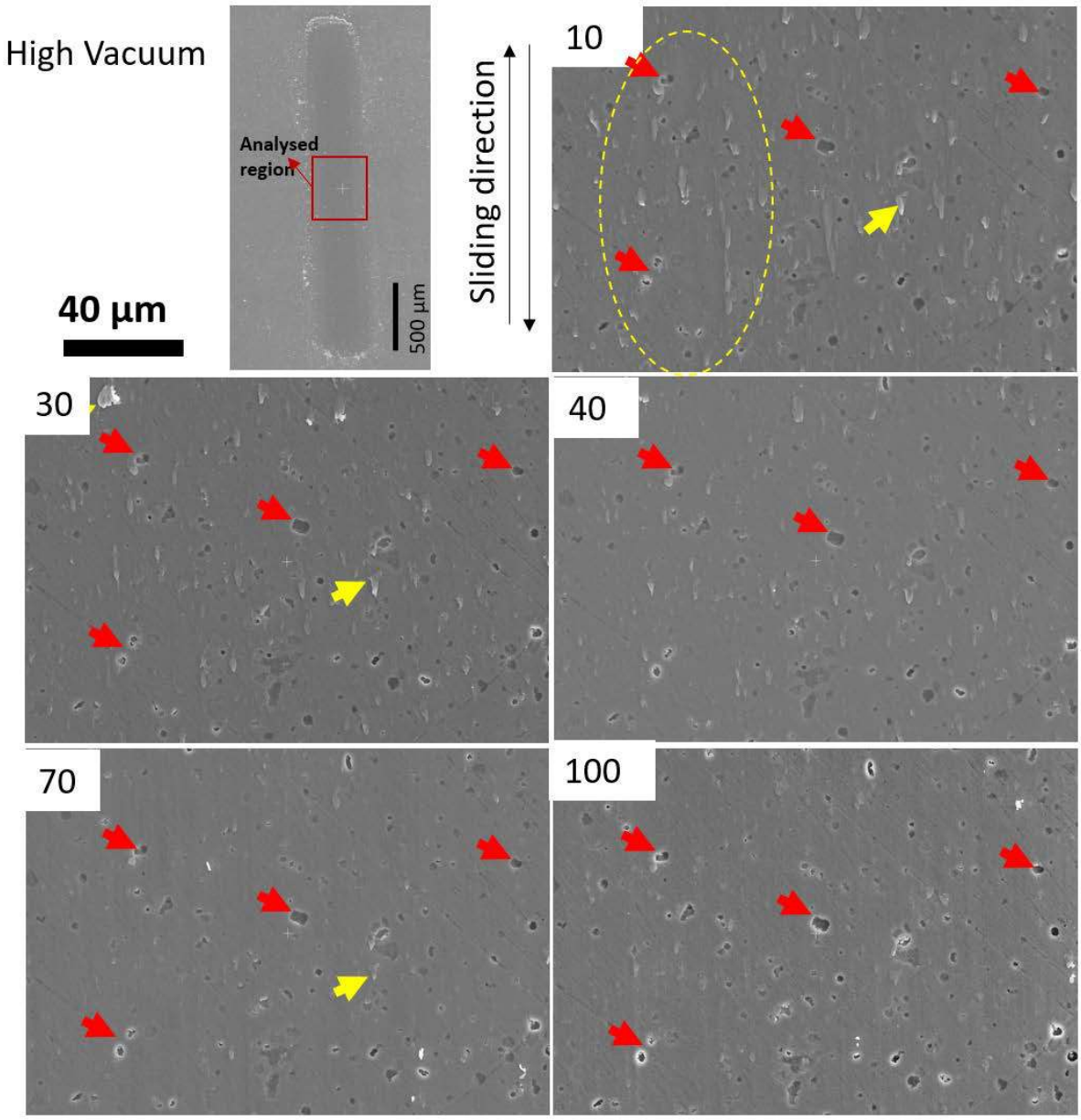


Figure 7: Center of the wear track after cycle 10, 30, 40, 70 and 100 in high vacuum tests

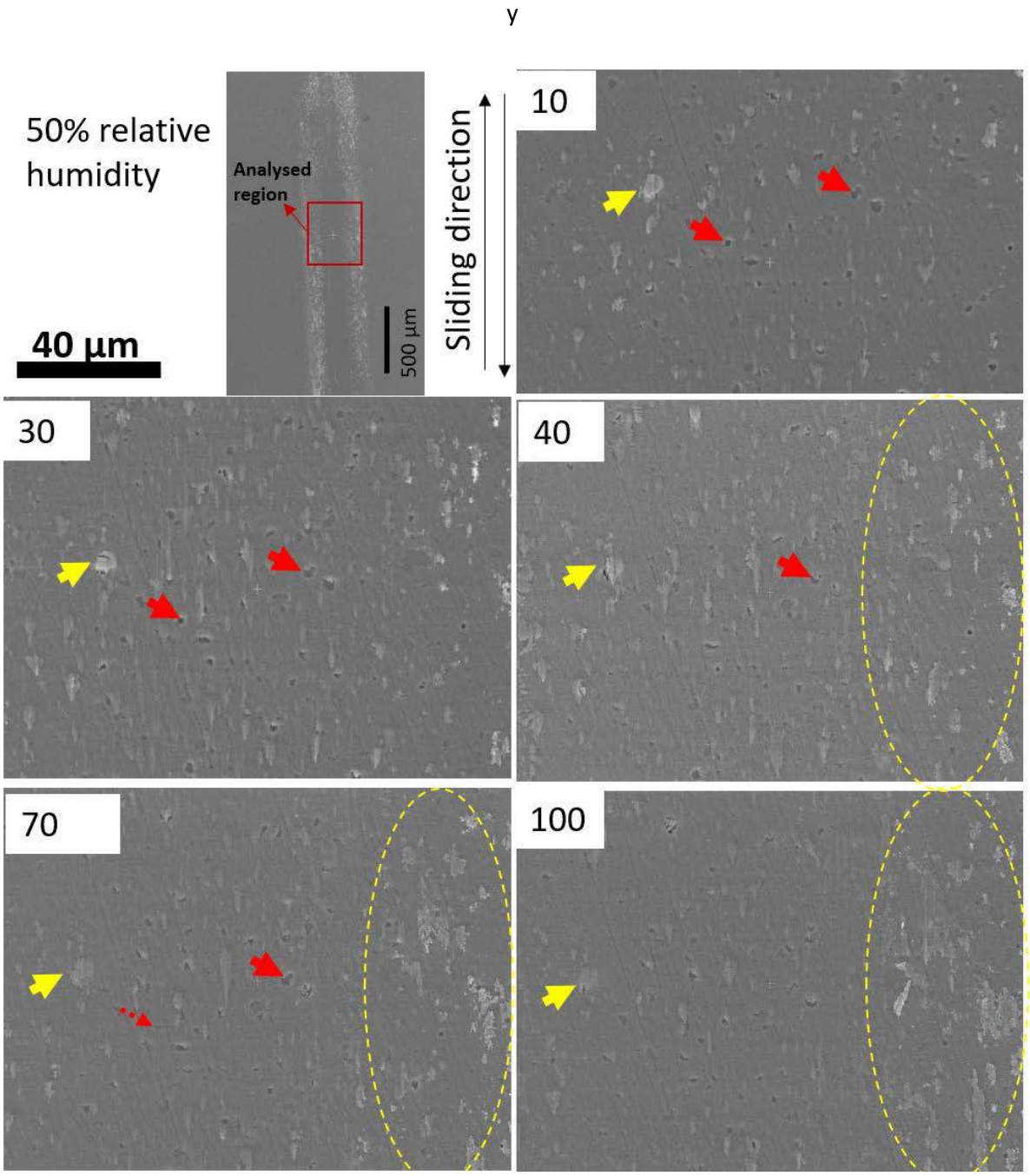


Figure 8: Center of the wear track after cycle 10, 30, 40, 70 and 100 in 50% RH tests

The mean friction coefficients of 100 cycles were compared with the evaluated wear tracks of TiN film both under high vacuum and 50% relative humidity by considering the SEM images. The difference of friction behavior observed in these two environments can be associated with differential arrangements of the particles, and different loss of debris. As a quantitative clue, it

was seen that the mean friction coefficient varied from 0.65 to 0.49 for high vacuum to humid environment.

3.2. *Post mortem* analysis

After 100 cycles, a microstructural characterization of wear tracks for the TiN film and the ball counter-face were investigated by SEM and EDS. Since the *in situ* analysis on the ball was not possible after venting the chamber, the ball was removed from the system for SEM observations leading to its superficial oxidation. SEM images report different ball track dimensions depending on the test environment, in agreement with the width of the films' wear tracks (Figure 9).

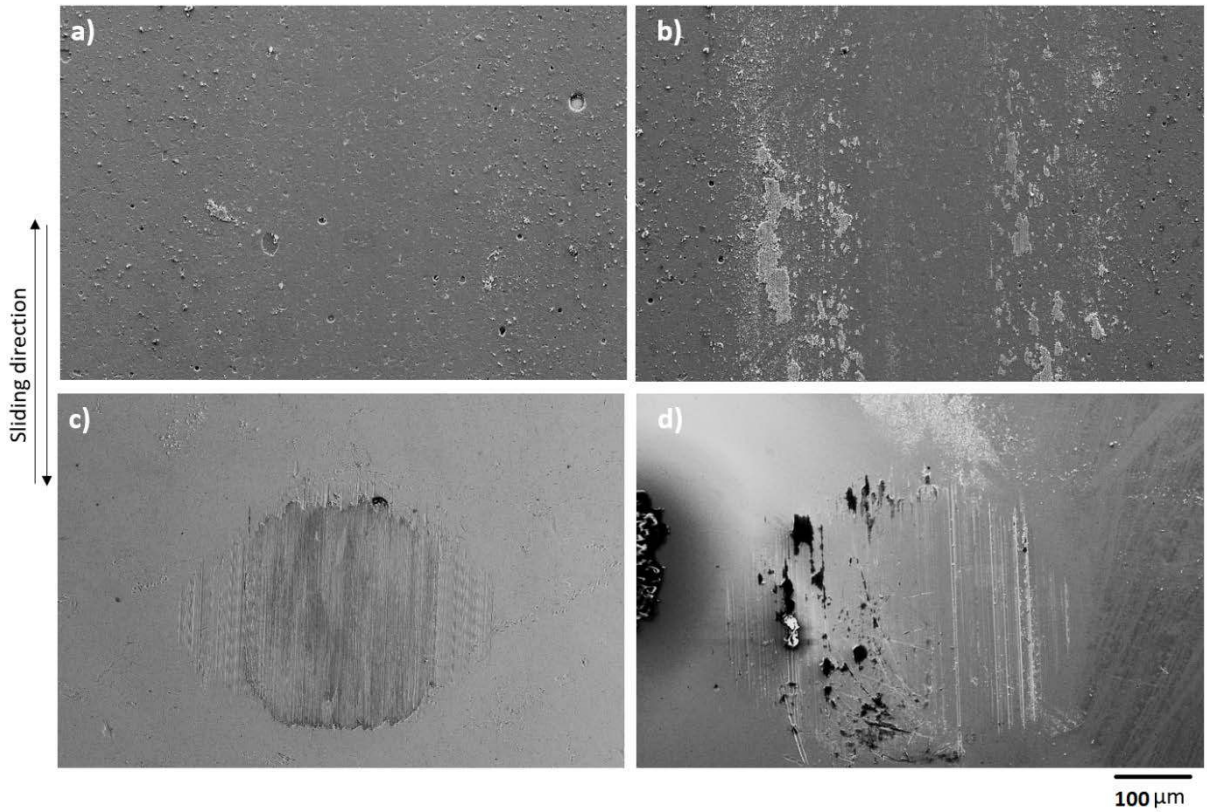


Figure 9: Comparison of wear tracks after 100 cycles for TiN film at a) high vacuum, b) 50% relative humidity, and balls tracks rubbed to TiN film at c) high vacuum, d) 50% relative humidity

After 100 cycles, wear tracks are well-defined, but show a strong heterogeneity. To have a global view of the wear track morphology, three characteristics zones were more specifically considered: both the extremities and the central area (Figure 10). Such specific points were selected to qualify the different regions of contact where the load is applied, where the sliding speed is constant, and where the sliding direction was changed. It appears quite compacted particles at the starting point of the contact in high vacuum conditions. On the other hand, in 50% relative humidity, particles seemed partially spread along the contact-starting region. There were also some debris along the track length. In addition, a large amount of third body particles are strongly compacted and formed a ductile film at the finishing point of the displacement length at humid environment by comparison with the high vacuum mode.

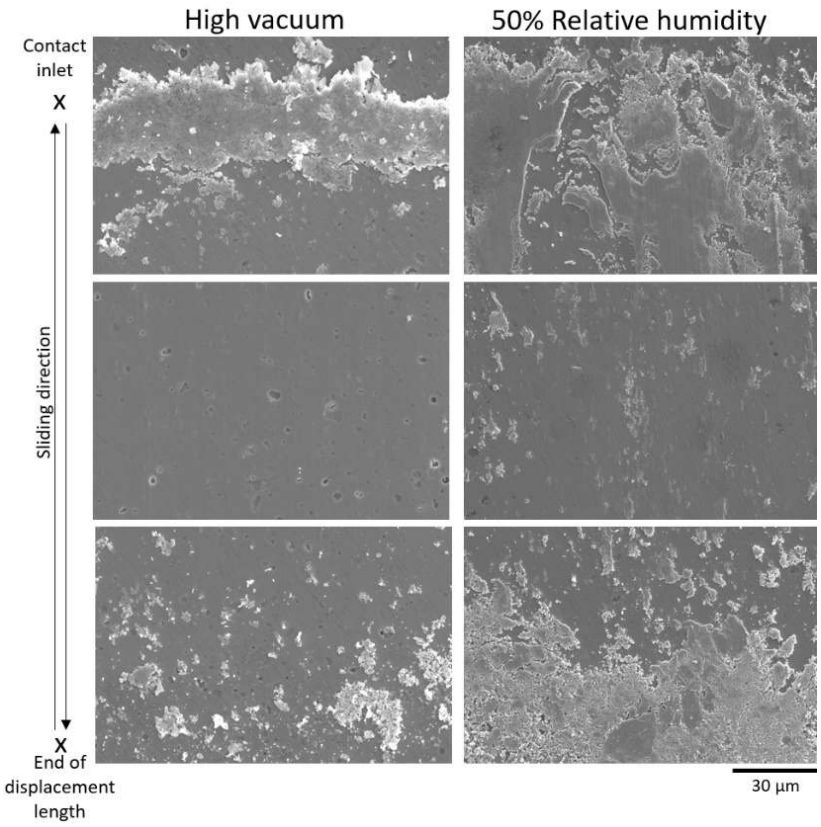


Figure 10: Wear track for 3 regions of interest after 100 cycles under high vacuum and 50% relative humidity

A complementary chemical analysis of the worn parts was carried by EDS for the coated flat sample after 100 cycles at the unloading-loading zone and at the center of the wear track (Figure 11). Titanium, iron, and oxygen were specifically analyzed: titanium signal reveals the nitride coating, while iron and oxygen indicate debris of the ball counter-part.

Whatever the environment, Ti distribution is inverted with Fe and O signals. Thus, at the tips of the wear track, debris are composed of iron oxide coming from the ball, compacted in the high vacuum test. In presence of relative humidity, the transferred material appeared more ductile and homogeneously distributed, as it is shown in the EDS maps. Also, when the centers of the wear tracks were investigated, small iron particles were detected at high vacuum (Figure 11b). However, these particles could be considered as from the ball since there is no significant film removal on this zone. On the other hand, there is a strong oxide signal in addition to detected iron on the frontiers of the wear track for the test performed in 50% relative humidity (Figure 11d). It could be stated that the iron oxide was spread over wear track in the humid environment.

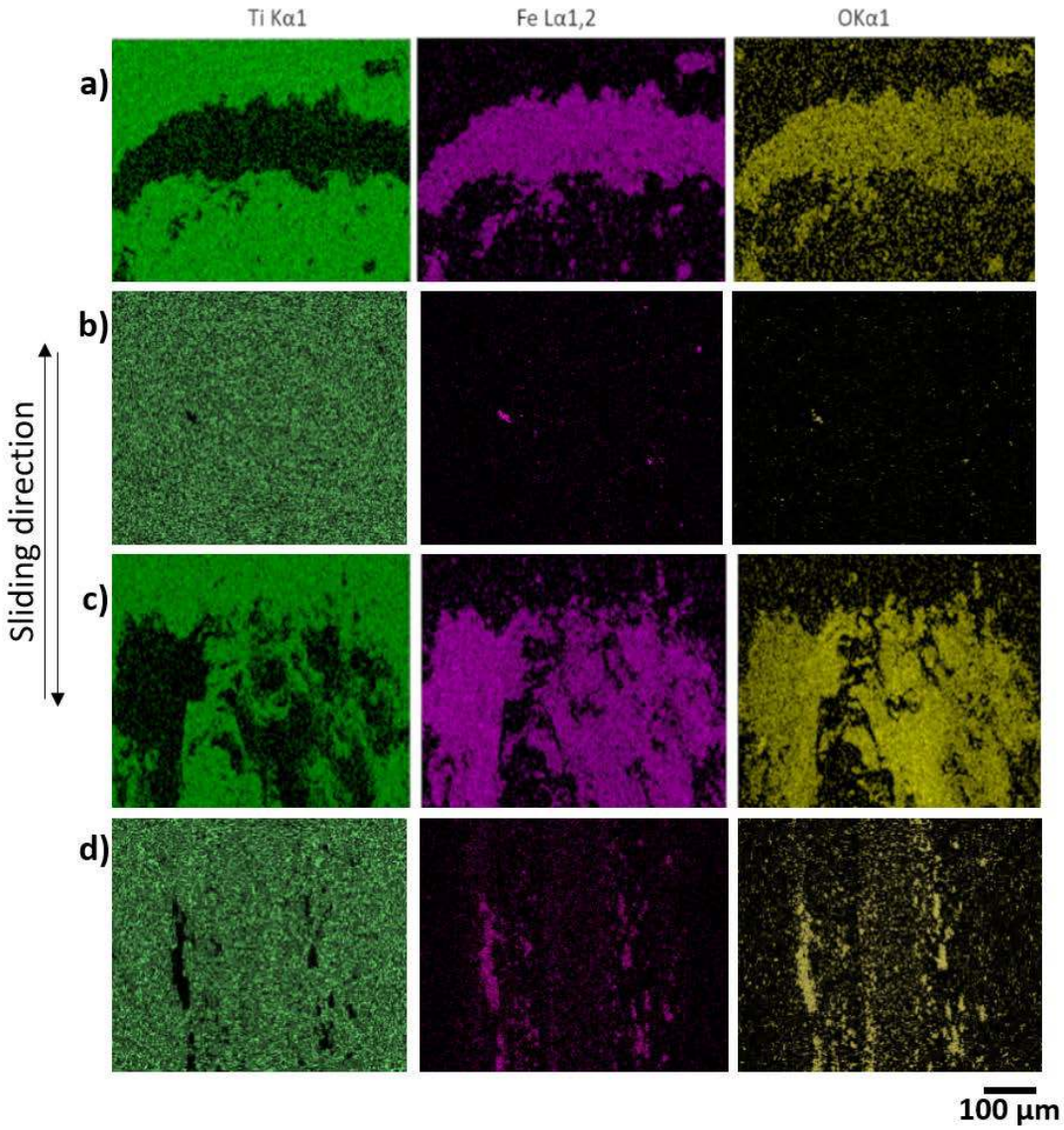


Figure 11: EDS maps of the worn TiN film after 100 cycles under at high vacuum from a) the starting of contact, b) center of the contact and at 50% relative humidity from c) starting of the contact, d) center of the contact

In addition to the previous phenomenological approach, a complementary quantitative study was also performed regarding topographic measurements. The damaged surface topography of the wear tracks of TiN film was scanned with a non-contact interferometer. Figure 12 shows 3D cross-sectional topographies and the surface profiles of the wear track after the test carried out in the two environments. The differences in the wear tracks could be seen in the 3D images extracted from the profile analysis.

Wear volumes were calculated as the average of 10 profiles indicated as the lines on the cross-section topographies in Figure 12. The reference unworn film surface has been defined as the 0 µm level. Thereby, the volume below the reference surface was considered as the worn material, while the volume above the reference surface was accepted as the accumulated particles along the frontiers of the wear track. When the gained volume was subtracted from the worn volume, the absolute wear volume was calculated. It was seen that the wear volumes were dependent on the atmosphere: it was higher for the wear track which has been generated in 50% of relative humidity (12762±41µm$^3$) than in high vacuum (9929±23 µm$^3$) test. It could be stated that even though the oxide layer formed on the wear track of the film caused a decrease of the friction coefficient, it leads to a higher wear volume.

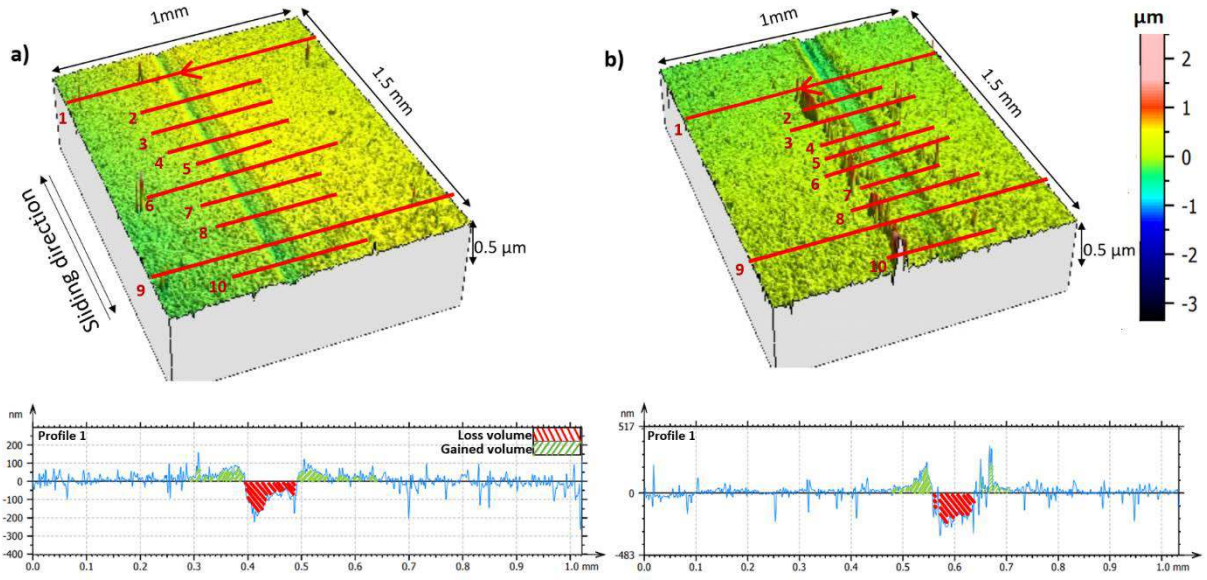


Figure 12: Wear track profiles from the beginning of the contact of TiN film with schema of wear volume calculation at a) high vacuum, b) 50% relative humidity

The same microstructural characterization was performed to the ball counter-face (Figure 13). Titanium was detected over the wear track on the ball surface at vacuum test, whereas almost no film material was detected on the surface of the ball used in humid mode. However, for the

high deformed region of the ball surface, more oxidation was evidenced due to the existence of water vapor at 50% humidity. The iron oxide seemed slightly higher in worn region for ball used in high vacuum test. Since the chamber had to be vented and the ball exposed to ambient air atmosphere, this higher oxidation in the worn zone could be related to an enhanced surface reactivity due to the fresh exposed worn metallic area. Such a local unexpected reactivity is often reported in tribo-corrosion experiments of passive materials [48]. On the other hand, in humid conditions, a more localized oxidation of the ball is detected on its extremities, without any traces of film transfer.

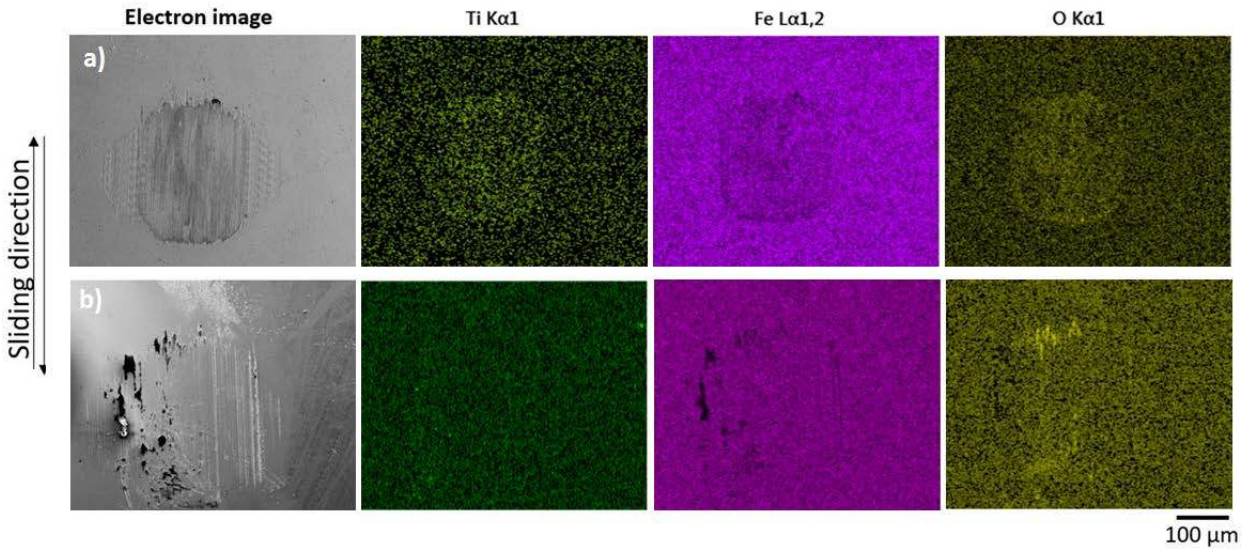


Figure 13: Electronic images and EDS maps acquired of the worn steel ball rubbed to TiN film for 100 cycles under a) high vacuum, b) 50% relative humidity

Moreover, profiles of the ball tracks were also characterized by non-contact interferometry (Figure 14). The surface of the ball rubbed to TiN film at 50% relative humidity-exhibits a slight visible flattening on the top. It has a rougher topography than high vacuum tests. This result is convenient with the wear tracks topographies and wear volumes calculated for respective environments.

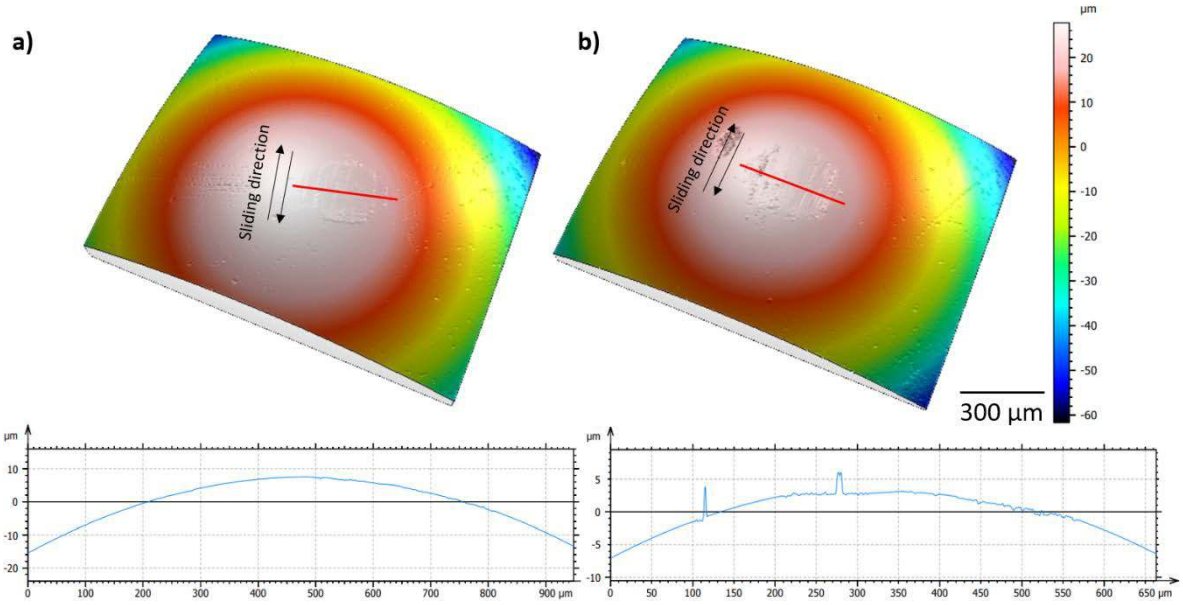


Figure 14: Wear tracks on balls rubbed to TiN film after 100 cycles at a) high vacuum, b) 50% relative humidity

## 4. Discussion

### 4.1. Role of the superficial TiN oxidation

The tribological behavior of thin TiN coating against a steel ball was studied at the mesoscale in different environments focusing on the run-in period. It was shown that the tribological behavior of materials involved in the contact and so their friction coefficients were influenced by the atmosphere. Moreover, the particles formed during the humid environment test were more spread and tend to be in crumbled form on the two turning points of the wear track. Under vacuum, particles were more localized and compact on the starting point of the contact of the wear track. Such a particles distribution could be correlated with the soft oxide layer formed on the wear track in humid environment, which was attested by the presence of oxygen by EDS analysis.

The role of humidity on the tribological behavior of TiN coatings has been highlighted in the literature. Yoon et *al.* [27] performed the tests on TiN films where the relative humidity was

tuned from 2% to 25% to 85% with steel balls. For the beginning of the tests, it was stated that while the friction coefficient was ~0.25 for the first 100 cycles at 2% and 25% relative humidity, it increased almost up to ~0.35 in 85% relative humidity test. However, with increasing number of cycles, lower friction coefficient was exhibited at 85% relative humidity than the rests performed in 2% and 25% humidity levels. The role of the titanium oxide corroborates the study of Zhang et *al.* on TiN films in dry and lubricated conditions. They indeed showed that the passive layer formed in humid environment on the contact area played the role of a solid lubrication film, decreasing the coefficient of friction [26]. As a confirmation, under high vacuum, the coefficient of friction was higher than under humidity, which can be interpreted by the impossibility for TiN to maintain and feed its superficial passive layer. It is worth mentioning that, there are only few studies about the friction behavior of TiN films under high vacuum. For instance, Chen et *al.* [39] have reported a lower mean coefficient of friction as 0.31 under vacuum (0.005 Pa) than in ambient air conditions which was 0.58 (at room temperature, 22-25% RH). Whereas, in our tests, the mean coefficient of friction was 0.75 in vacuum and it decreased to 0.49 for the test performed in 50% RH. These results were defined as unusual also in their study and it was explained by the mechanical polishing of the film surface during the sliding process, which caused a reduction of the surface roughness lowering the coefficient of friction. Nevertheless, their films were unusually thick (10.3 μm) and much higher than ours (2.3 μm) in addition to the longer displacement length that they selected for their procedure. This difference in thickness and displacement may affect also the final surface roughness of TiN films between two studies, which may contribute to explain the two differential sliding regimes.

4.2. Effect of unloading-reloading process: Role of debris dynamics

To perform *in situ* analyses, a procedure involving successive loading and unloading of the system was required. This procedure caused a relatively lowered mean COF for the first cycle

of each set, with an increasing trend for the following cycles in the same set (Figure 5). This issue explains why the both extremities of the wear track, where particles accumulate, is dissymmetric, highlighting by the different distribution and volume of the particles.

In order to estimate influence of the transitory loading-unloading steps, a 100-cycles test was performed in a single run without any opening of the contact. Evolution of the mean COF with respect to the cycle number appears in figure 15. The COF in humid conditions is quite stable around 0.40 which is very close to the value of the contact-interrupted *in situ* test (Figure 5). However, the tribological response recorded under high vacuum is much more complex, with a continuous increase of the COF from 0.45 to 0.90 for the 35 first cycles, strictly similar to the one reported in Figure 5. Then, from 40 to 60 cycles, the evolution is drastically changed with a slight decrease of the COF, which can be attributed to trapping of debris and then ejection of them after cycle 60. Finally, a scattered regime is initiated, with fluctuating values reaching 1.0 to 1.10. Such an evolution suggests a modification of the nature of the contact during the test, reaching a steel-steel contact.

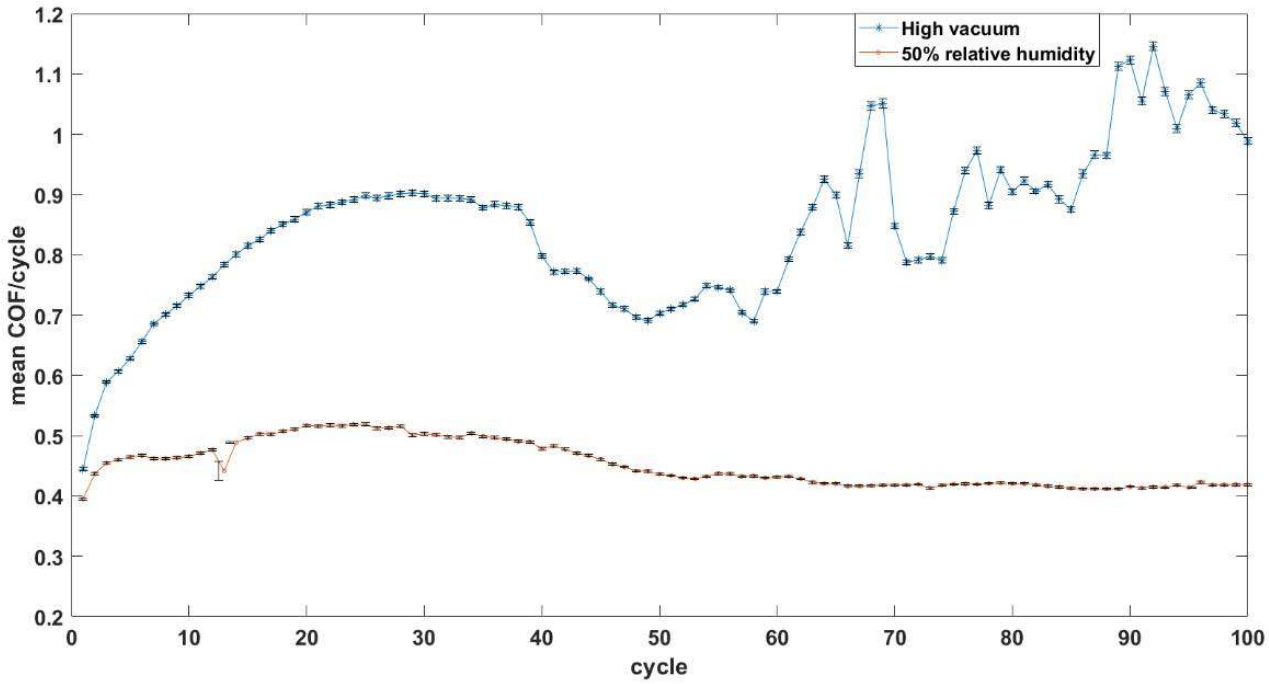

Figure 15: Evolution of the mean coefficient of friction for the tests carried out in a single run (without successive opening of the contact) for 100 cycles at high vacuum and 50% relative humidity tests.

Under vacuum, the EDX analysis of the wear track (figure 16a) confirmed that the uninterrupted test has led to the total removing of the nitride coating, and the underlying steel substrate appearing. On ball track, an important transfer of TiN and large amount of particles or agglomerates of TiN were also highlighted in the center (figure 16c). These debris are accumulated at edges of the track, but also stacked to the ball center, which highlighted that some TiN debris were trapped in the contact. In the loading-unloading configuration, each successive unloading of the contact led to a significant loss of released debris, resulting in an under-estimated reduced wear. In opposite, in the case of the uninterrupted test under vacuum, debris are emitted during the first 35 cycles and are trapped in the contact area, leading to a higher damage of the coating until its total consumption.

For the test conducted under 50% relative humidity, the film remained whatever the protocol adopted: with or without contact opening. Traces of iron oxides are detected all along the track coming from the ball (figure 16b). Chemical analysis of the ball track highlighted a local oxidation of the ball contact region under humid environment (Figure 16d). The beneficial effect of the humidity on the sliding conditions, already revealed in the loading-unloading configuration, is confirmed. That confirms the protective role of the passive layer formed under relative humidity.

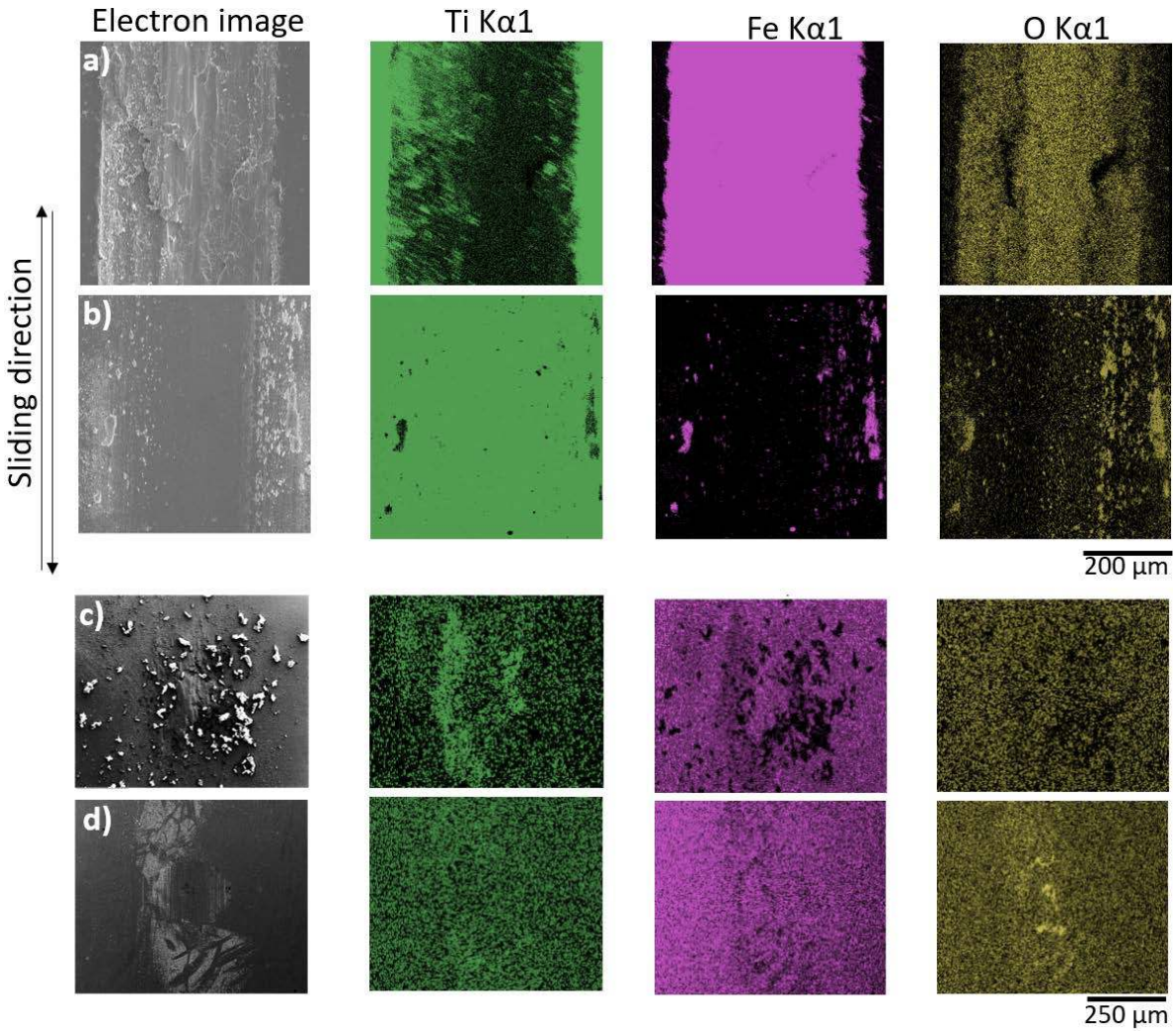


Figure 16: EDS Maps after uninterrupted test. Wear track under a) high vacuum, b) 50% relative humidity and ball track under c) high vacuum, d) 50% relative humidity

4.3. Towards a mechanism of degradation

Combining the evolution of COF in both configurations, with contact opening (Figure 5) or as uninterrupted (Figure 15), the morphology and the chemical nature of wear tracks, it is possible to propose a mechanism degradation highlighting the role of environment on the one hand, and the dynamics of debris on the other hand. The results can be revisited in the light of the tribological circuit [17] which describes the different third body flows that may take place in a contact. The source flow (Qs) corresponds to the detachment of particles due to tribological transformations of the structure or damage mechanisms such as cracking, abrasion… It leads to

the formation of the third body. The internal flow is the flow of the third body circulating inside the contact. The recirculation flow (Qr) is composed of the third body escapes from the contact and reintroduced into the contact. Wear flow (Qw), is composed of the third body (wear debris) that has been definitively ejected from the contact and can no longer participate in velocity accommodation. The wear rate is defined through a balance between the particles formation flow (Qs) and the particles ejection flow (Qe) from the contact [49].

Schemas presented in Figure 17 illustrate the evolution of the contact area throughout the continuous test, highlighting the nature of interfaces involved in the contact.

Under vacuum, the debris at the edges of the wear track are constituted from iron and titanium, meaning that source flow of particles come from the ball and the coating. The accumulation of those debris at the edges, *e.g.* outside of the contact, highlighted that wear flow has been activated. The particles trapped in the contact contributed to the internal flow and caused changes on the friction response of the film. Such hard debris would act as abrasive matter. In the loading-unloading configuration, those debris can be lost for the contact because of the opening procedure and a new contact steel – TiN is occurred without such debris (the coating is still visible after each 10 cycles, (Figure 6)). Even if the source flow is reactivated to form new debris, the ejection of debris at next opening (wear flow) prevent the abrasion. In the single run configuration, debris were trapped, preventing this cyclic phenomenon but allowing abrasion by activation of the internal flow, causing a dramatic wear of the coating (Figure 17c), until reaching the substrate itself (Figure 17d).

At 50% relative humidity, the agglomerates and debris spread on the surfaces (figures 7 and 10), which highlights the plastic flow of the third body. Besides, the film was preserved throughout the 100 cycles. Under humidity, the nature of the coating surface is different than under vacuum, and present an initial passive titanium oxide layer. Such top layer, in contact with the ball, is soft. Source flow is constituted by particles detached from the coating (presence

of Ti) and thus of this passive layer and by particles detached from the ball (presence of iron). The accumulation of particles at the edges and some debris along the track length, *e.g.* outside the contact, highlighted that wear flow has been activated. The third body present in the contact spread on the surface, and contributed to the internal flow. Its ductility facilitates is entrapment for whatever the configuration. The wear flow is not increased between the two configurations. Furthermore, the water vapor environment is prone to continuously feed and renew the passive layer, which would be on the basis of the stable and lower COF values with time compared to those under vacuum.

The small-scale tribological investigation adopted in this study was then able to explain the beneficial solid-lubricant role of titanium oxide reported in the literature, and in this sense has validated our approach together with the mini-tribometer.

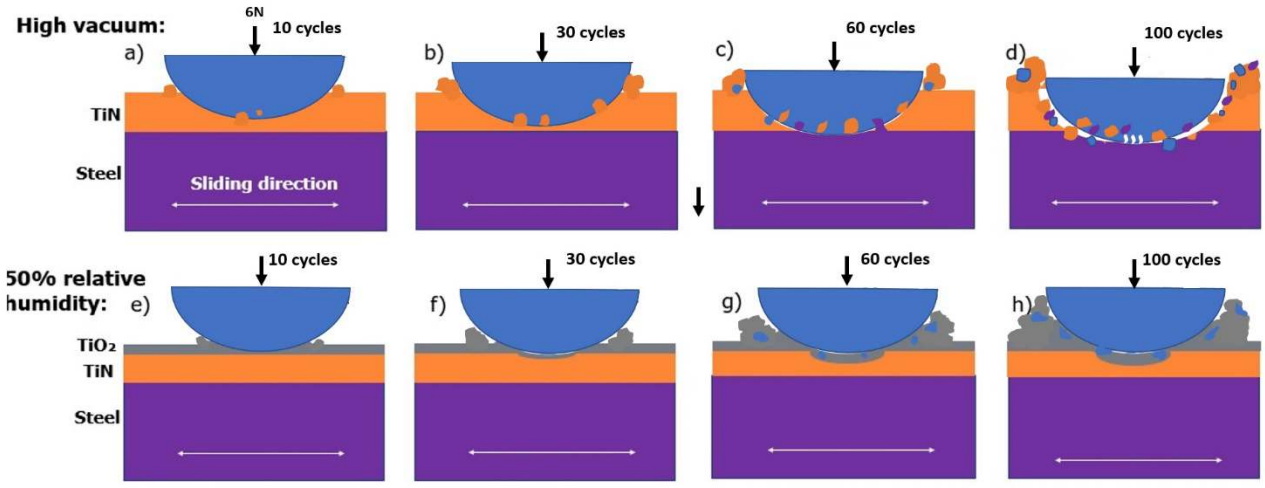


Figure 17: Schematic representation of the damaging mechanism of TiN-coated steel under a-d) high vacuum, or e-h) 50% relative humidity.

*(The scale of balls and films thickness are not adapted to emphasize the deformation on both film and ball surfaces clearly)*

**Conclusion**

To sum up, *in situ* characterization of a model-TiN film was performed during the run-in period with a custom-built reciprocating mini-tribometer. This device can be introduced into the chamber of an environmental SEM, to analyze the effect of the environment on the tribological behavior of materials at small scale. The main experimental parameters; loading, displacement characteristics and nature of the environment are controlled, while the COF is continuously measured. Morphology of the film wear track is recorded *in situ* throughout the tribo-test. A *post mortem* evaluation of the worn damaged volume was also done on both counterparts, together with a morphological and chemical characterization of wear tracks.

To validate this device, a model-contact was investigated as a proof-of-concept: a PVD micrometric TiN film rubbing onto a hard steel ball. The relevance, repeatability and efficiency of the mini-tribometer were demonstrated by comparison with sliding values got with more conventional tribometers.

It was shown that degradation mechanisms of TiN were strongly dependent on its use environment: the role of humidity, which allowed a continuous growth of oxide layer favoring the sliding was confirmed, while it was demonstrated that the wear of TiN under vacuum was rather governed by the dynamic of abrasive debris (third body flows).

Unfortunately, a real-time chemical characterization of the wear track was not possible with the current configuration. This next step can be achieved either by performing EDX analysis *in situ* in SEM, or by using a transparent ball, allowing a continuous analysis of the contact by Raman spectroscopy.

**Acknowledgments**

This work was supported by the LABEX MANUTECH-SISE (ANR-10-LABX-0075) of Université de Lyon, within the Plan France 2030 operated by the French National Research Agency (ANR). Authors also acknowledge the CLYM platform (www.clym.fr), for giving

access to the dedicated environmental SEM Quattro (ThermoFischer Scientific). The authors would like to thank gratefully J. Ferreira, Ch. Goudin, N. Filaire and P. Chen for their technical involvement for the tribometer design.

## References

[1] P. Kapsa, Tribology at Different Scales, *Advanced Engineering Materials. 3*(8) (2001) 531. doi:10.1002/1527-2648(200108)3:8<531:aid-adem531>3.0.co;2-1.

[2] Y. Berthier, Handbook of Materials Behavior Models, Acad.Press, Lemaître, 2001, pp. 676–699.

[3] W. G. Sawyer, K. J. Wahl, Accessing Inaccessible Interfaces: In Situ Approaches to Materials Tribology, *MRS Bulletin, 33*(12), 1145-1150. (2008) doi:10.1557/mrs2008.244.

[4] M. Kosinskiy, S. I. Ahmed, Y. Liu, J. A. Schaefer A compact reciprocating vacuum microtribometer. *Tribology International, 56*, (2012) 81-88. doi:10.1016/j.triboint.2012.06.019.

[5] M. J. Cordill, P. Kreiml, C. Mitterer, Materials Engineering for Flexible metallic thin film applications, *Materials*, *15*(3), (2022) 926. https://doi.org/10.3390/ma15030926.

[6] P. Stoyanov, R. Chromik, Scaling Effects on Materials Tribology: From Macro to Micro Scale, *Materials, 10*(5), (2017) 550. doi:10.3390/ma10050550.

[7] D. D. Kumar, N. Kumar, S. Kalaiselvam., S. Dash, R. Jayavel, Micro-tribo-mechanical properties of nanocrystalline TiN thin films for small scale device applications, *Tribology International, 88*, (2015) 25-30. doi:10.1016/j.triboint.2015.02.031.

[8] B. Bhushan, Tribology on the macroscale to nano-scale of microelectromechanical system materials: A review, *Proceedings of the Institution of Mechanical Engineers, Part J: Journal of Engineering Tribology, 215*(1), (2001) 1-18. doi:10.1243/1350650011541657.

[9] M. Gee, J. Nunn, A. Muniz-Piniella, L. Orkney, Micro-tribology experiments on engineering coatings, *Wear, 271*(9-10), (2011) 2673-2680. doi:10.1016/j.wear.2011.02.031.

[10] C. C. Schmitt, J. R. Elings, M. Serry, Nanoindenting, Scratching and Wear Testing with the Atomic Force Microscopy, Bruker (2010).

[11] Y. G. Gogotsi, A. Kailer, K. G. Nickel, Phase transformations in materials studied by micro-raman spectroscopy of indentations, *Materials Research Innovations*, *1*(1), (1997) 3–9. https://doi.org/10.1007/s100190050011.

[12] A. V. Desai & M. A. Haque, A novel MEMS nano-tribometer for dynamic testing in-situ in Sem and Tem. *Tribology Letters*, *18*(1), (2005), 13–19. https://doi.org/10.1007/s11249-004-1700-z

[13] T. D. Jacobs, C. Greiner, K. J. Wahl, R. W. Carpick, Insights into tribology from in situ nano-scale experiments, *MRS Bulletin, 44*(06), (2019) 478-486. doi:10.1557/mrs.2019.122.

[14] J. Heinrichs,, M. Olsson, I. Z. Jenei, S. Jacobson, Transfer of titanium in sliding contacts—New discoveries and insights revealed by in situ studies in the SEM, *Wear, 315*(1-2), (2014) 87-94. doi:10.1016/j.wear.2014.04.006.

[15] J. Heinrichs, M. Olsson, S. Jacobson, Mechanisms of material transfer studied in situ in the SEM, *Wear, 292-293*, (2012) 49-60. doi:10.1016/j.wear.2012.05.033.

[16] W. Federle, T. Endlein, Locomotion and adhesion: Dynamic control of adhesive surface contact in ants, *Arthropod Structure & Development, 33*(1), (2004) 67-75. doi:10.1016/j.asd.2003.11.001.

[17] J. Heinrichs, M. Olsson, S. Jacobson, Influence of tool steel microstructure on initial material transfer in metal forming—In situ studies in the SEM, *Wear, 302*(1-2), (2013) 1249-1256. doi:10.1016/j.wear.2013.01.114.

[18] A. P. Merkle, L. D. Marks, Liquid-like tribology of gold studied by in situ TEM, *Wear, 265*(11-12), (2008) 1864-1869. doi:10.1016/j.wear.2008.04.032.

[19] S. Descartes, Y. Berthier, Rheology and flows of solid third bodies: Background and application to an MoS1.6 coating, *Wear, 252*(7-8), (2002) 546-556. doi:10.1016/s0043-1648(02)00008-x.

[20] J. Martin, T. L. Mogne, M. Boehm, C. Grossiord, Tribochemistry in the analytical UHV tribometer, *Tribology International, 32*(11), (1999) 617-626. doi:10.1016/s0301-679x(99)00090-0.

[21] J. M. Shockley, S. Descartes, P. Vo, E. Irissou, R. R. Chromik, The influence of al2o3 particle morphology on the coating formation and dry sliding wear behavior of cold sprayed al–al2o3 composites, *Surface and Coatings Technology*, *270*, (2015) 324–333. https://doi.org/10.1016/j.surfcoat.2015.01.057 .

[22] S. Descartes, L. Courtieux, Y. Berthier, F. Peditto, Tribological study of Oral Care Silica, *Tribology International*, *82*, (2015) 551–560. https://doi.org/10.1016/j.triboint.2014.02.023.

[23] J. R. Waldrop, Titanium nitride schottky-barrier contacts to gaas. *Applied Physics Letters*, *43*(1), (1983) 87–89. https://doi.org/10.1063/1.94131.

[24] C. Muratore, J. E. Bultman, S. M. Aouadi, A. A. Voevodin, In situ raman spectroscopy for examination of high temperature tribological processes, *Wear*, *270*(3-4), (2011) 140–145. https://doi.org/10.1016/j.wear.2010.07.012.

[25] B. Murarash & M. Varenberg, Tribometer for in situ scanning electron microscopy of microstructured contacts. *Tribology Letters*, *41*(2), (2010), 319–323. https://doi.org/10.1007/s11249-010-9717-y

[26] Y. Naerheim, A SEM/AES/XPS tribometer for rolling and sliding contacts. *Wear*, *162-164*, (1993), 593–596. https://doi.org/10.1016/0043-1648(93)90547-y

[27] B. Meylan, D. Ciani, B. Zhang, E. Cuche & K. Wasmer, A new ball-on-disk vacuum tribometer with *in situ* measurement of the wear track by Digital Holographic Microscopy. *Surface Topography: Metrology and Properties*, *5*(4), (2017), 044004. https://doi.org/10.1088/2051-672x/aa854a

[28] C. Chen, P. Xue, X. Fan, C. Wang & D. Diao, Friction-induced rapid restructuring of graphene nanocrystallite cap layer at sliding surfaces: Short run-in period. *Carbon*, *130*, (2018) 215–221. https://doi.org/10.1016/j.carbon.2018.01.022

[29] R. R. Chromik, A. L. Winfrey, J. Lüning, R. J. Nemanich & K. J. Wahl, Run-in behavior of Nanocrystalline Diamond Coatings studied by in situ tribometry. *Wear*, *265*(3-4), (2008), 477–489. https://doi.org/10.1016/j.wear.2007.11.023

[30] M. J. Marino, E. Hsiao, Y. Chen, O. L. Eryilmaz, A. Erdemir & S. H. Kim, Understanding run-in behavior of diamond-like carbon friction and preventing diamond-like carbon wear in humid air. *Langmuir*, *27*(20), (2011), 12702–12708. https://doi.org/10.1021/la202927v

[31] T. W. Scharf, & I. L. Singer, Role of the transfer film on the friction and wear of metal carbide reinforced amorphous carbon coatings during run-in. *Tribology Letters*, *36*(1), (2009), 43–53. https://doi.org/10.1007/s11249-009-9457-z

[32] J. Michael, S. Prasad, J. Jungk, M. J. Cordill, D. Bammann, C. Battaile, N. Moody, B. Majumdar, Modeling of friction-induced deformation and microstructures, (2016) https://doi.org/10.2172/902880.

[33] P.J. Blau, On the nature of running-in. *Tribology International*, *38*(11-12), (2005), 1007–1012. https://doi.org/10.1016/j.triboint.2005.07.020

[34] M. Sasaki, I. Nakamura, I. Takano, Y. Sawada, Vacuum pressure dependence of the tribological properties of Ti, TiO2, and TiN thin films, *Electrical Engineering in Japan, 149*(3), (2004) 1-7. doi:10.1002/eej.20020.

[35] Q. Chen, A. Li, G. Wu, Z. Lu, G. Zhang, G. Tian, Structure vs chemistry: Tribological behavior of TiN films in the nitrogen atmosphere, *Ceramics International, 46*(18), (2020) 28053-28063. doi:10.1016/j.ceramint.2020.07.300.

[36] L. Zhang, H. Yang, X. Pang, K. Gao, H. T. Tran, A. A. Volinsky, TiN-Coating Effects on Stainless Steel Tribological Behavior Under Dry and Lubricated Conditions, *Journal of Materials Engineering and Performance, 23*(4), (2014) 1263-1269. doi:10.1007/s11665-014-0904-0.

[37] S. Yoon, M. Kang, S. Kwon, K. H. Kim, The influence of counterface materials and humidity on the tribological behavior of arc ion plated TiN films, *Surface and Coatings Technology, 157*(2-3), (2002) 144-150. doi:10.1016/s0257-8972(02)00145-7.

[38] A. Gant, M. Gee, L. Orkney, The wear and friction behaviour of engineering coatings in ambient air and dry nitrogen, *Wear, 271*(9-10), (2011), 2164-2175. doi:10.1016/j.wear.2011.02.032.

[39] Q. Chen, G. Wu, D. Li, A. Li, L. Shang, Z. Lu, Z. Zhang, Z. Wu, G. Tian, Understanding the unusual friction behavior of TiN films in vacuum, *Tribology International, 137*, (2019) 379-386. doi:10.1016/j.triboint.2019.05.024.

[40] M. Gee, T. Kamps, P. Woolliams, J. Nunn, K. Mingard, In situ real time observation of tribological behaviour of coatings, *Surface and Coatings Technology*, *442*, (2022) 128233. https://doi.org/10.1016/j.surfcoat.2022.128233.

[41] D. J. Stokes, Characterisation of soft condensed matter and delicate materials using environmental scanning electron microscopy (ESEM), *Advanced Engineering Materials*, *3*(3), (2001) 126–130. https://doi.org/10.1002/1527-2648(200103)3:3<126::aid-adem126>3.0.co;2-b.

[42] L. F. Lu, H. Y. Chen, Characterization of titanium nitride films deposited by cathodic arc plasma technique on copper substrates, *Surface and Coatings Technology*, *130*(2-3), (2000) 290–296. https://doi.org/10.1016/s0257-8972(00)00710-6.

[43] M. A. Hussein, A. Y. Adesina, A. M. Kumar, A. A. Sorour, N. Ankah, N. Al-Aqeeli, Mechanical, in-vitro corrosion, and tribological characteristics of TiN coating produced by cathodic arc physical vapor deposition on Ti20nb13zr alloy for biomedical applications, *Thin Solid Films*, *709*, (2020) 138183. https://doi.org/10.1016/j.tsf.2020.138183.

[44] A. Mège-Revil, P. Steyer, G. Thollet, R. Chiriac, C. Sigala, J. C. Sanchéz-Lopéz, C. Esnouf, Thermogravimetric and in situ sem characterisation of the oxidation phenomena of protective nanocomposite nitride films deposited on steel, *Surface and Coatings Technology*, *204*(6-7), (2004) 893–901. https://doi.org/10.1016/j.surfcoat.2009.06.040.

[45] P. Steyer, A. Mege, D. Pech, C. Mendibide, J. Fontaine, J. F. Pierson, C. Esnouf, P. Goudeau, Influence of the nanostructuration of PVD Hard Tin-based films on the durability of Coated Steel, *Surface and Coatings Technology*, *202*(11), (2008) 2268–2277. https://doi.org/10.1016/j.surfcoat.2007.08.073.

[46] V. Chawla, R. Jayaganthan, R. Chandra, Microstructural characteristics and mechanical properties of magnetron sputtered nanocrystalline tin films on glass substrate, *Bulletin of Materials Science*, *32*(2), (2009) 117–123. https://doi.org/10.1007/s12034-009-0018-8.

[47] T. Namazu, S. Inoue, H. Takemoto, K. Koterazawa, Mechanical properties of polycrystalline titanium nitride films measured by XRD tensile testing, *IEEJ Transactions on Sensors and Micromachines*, *125*(9), (2005) 374–379. https://doi.org/10.1541/ieejsmas.125.374.

[48] K. Kim, J. Geringer, J. Pellier, D. D. Macdonald, Fretting corrosion damage of total hip prosthesis: Friction coefficient and damage rate constant approach, *Tribology International*, *60*, (2013) 10–18. https://doi.org/10.1016/j.triboint.2012.10.008.

[49] N. Fillot, I. Iordanoff, Y. Berthier, Modelling third body flows with a discrete element method—a tool for understanding wear with adhesive particles, *Tribology International*, 40, (2007) 973–981. doi:10.1016/j.triboint.2006.02.056.